A Novel Underactuated Continuum Robot with Shape Memory Alloy Clutches

Christopher Bishop, Matteo Russo, *Member*, *IEEE*, Xin Dong, and Dragos Axinte

***Abstract*—The many degrees of freedom of continuum robots (CRs) enable unique applications in the search and rescue, medical and aerospace industries. However, the many motors required result in unwieldy external actuation packs and additional weight. Underactuation can achieve any pose with four motors by locking sections through clutching of cables. Existing underactuated solutions are characterized by lengthy joint locking times, add significant weight and are not scalable. In this work, a novel design and motion strategy is introduced, with shape memory alloy (SMA) wires to control clutches that lock cables for section locking. In addition to using conventional smooth cables, beaded cables are proposed for improved clutching strength. The workspace of the design is analyzed, and design tools are proposed to optimize bead pitch. Finally, the operation of the proposed underactuated CR is demonstrated on a prototype that achieves a mean repeatability of 1.41mm, equivalent to 0.43% of the backbone length. Section locking is achieved in 1 second and section unlocking is achieved in 5 seconds.**

***Index Terms*—Continuum Robot, Underactuation, Modular Robots, Shape Memory Alloy**

I. Introduction

CONTINUUM robots are snake-like bioinspired designs that can bend in a continuous way. This means that they are highly flexible and can navigate in cluttered environments such as gas turbines [1], [2], nuclear facilities [3], [4], and the human body [5]. Multiple design solutions have been proposed since the 1960s, [6], [7], the majority of which belong to the following three categories: external actuation [8], [9], [10] intrinsic actuation [11], [12], and concentric tubes [13], [14], [15]. CRs with intrinsic actuation have actuators embedded in the snake body structure, resulting in heavy and bulky designs with higher payloads but with a reduced inner lumen for the delivery of tools to the tip. For this reason, they are suited to applications in large environments, such as nuclear plants, but they cannot navigate in narrow complex geometries, such as aeroengines. Concentric tube CRs consist of hollow cylinders with constant curvature when relaxed, arranged telescopically. Each tube in a concentric tube CR can rotate and move axially to maneuver the robot about its workspace. Concentric tube CRs have advantageously small diameters but are limited by their small payload and reduced reach.

Externally actuated CRs have an actuation pack outside the body of the robot that is beneficial for decreasing the robot's diameter while maintaining a substantial payload. These robots are usually tendon-driven, and three or more cables are required to control two degrees of freedom (DoF) per each independent section of the robot [16]. This solution limits the number of sections that a CR can have, as cables are routed through the body of the whole robot. Thus, the sections that are closer to the actuation unit, later referred to as the proximal sections, require all the cables to pass through them, increasing the minimum size of each disk. Further, CRs are not modular designs: if more DoFs are needed, the number of sections cannot be changed without redesigning both the actuation pack and the body of the robot. As the DoFs of a cable-driven CR increase, so does the complexity of their control algorithm and the bulkiness of their actuation packs, which become increasingly unwieldy and limits deployment in confined spaces [17].

Aside from the size and actuation limitations, a third issue affects the control of these CRs. As the cables that drive the sections near the tip of the robot, called distal sections, pass through the whole robot, the tension required to maintain the position of the proximal sections depends on the configuration of the whole system. Furthermore, the stiffness varies as the distal cables exert forces along the arm [18], [19].

A solution to the large actuation packs and the limited space for cables is to underactuate the CR. Reconfigurable actuation packs have been proposed to actuate multiple cables with a single motor operating alternatively on them [20]. However, the number of cables required still sets an upper limit on the robot length to diameter ratio. Thus, reconfigurable actuation packs do not solve the cross-section space limitation, i.e., as more sections are added the total number of cables required increases.

Conversely, by partially locking the configuration of the robot, in principle, any pose can be realized with as few as three actuating cables, unlocking the sections one by one and moving them independently from the others. As summarized in Table I, two methods to constrain the motion of a section have been widely used in scientific literature: locking the shape of the section by stiffening (jamming or phase transition), or clutching the cables running through a section to prevent its motion.

Filling sections with phase changing material is a common locking solution, as shown in [21], [22], [23]. Shape memory polymers (SMP) have been used to lock sections of underactuated (UA) 2D snake robots [21]. The reported activation and relaxation time is 15 seconds which is notably longer than the approximate 1s activation typical of SMAs [24].

Submitted for review on 24/01/2022; revised 19/05/2022; accepted 22/05/2022.

Corresponding author: Dragos Axinte (dragos.axinte@nottingham.ac.uk)

This work was supported by UK EPSRC Industrial CASE (ICASE) studentship and Rolls-Royce.

C. Bishop, M. Russo, X. Dong, and D. Axinte are with the Rolls-Royce UTC in Manufacturing and On-Wing Technology, Faculty of Engineering, University of Nottingham, Nottingham NG8 1BB, United Kingdom (e-mail: {christopher.bishop; matteo.russo; xin.dong; dragos.axinte} @nottingham.ac.uk).

Furthermore, the presence of additional material on the passive part of the snake decreases flexibility and increases weight, and the buckling on the SMP might interfere with the backbone curvature in 3D operation. Likewise, a low melting point alloy (LMPA) for section locking [22] occupies a large amount of space on the robot, increases weight and is characterized by long heating and cooling times (177 seconds).

In the example in [25], an underactuated CR for minimally invasive surgery relies on two concentric robots which can switch between two stiffness states, compliant and rigid, controlled with cable tensioning. However, proximal sections cannot be moved without completely withdrawing the robot from the workspace. A similar concept, presented in [26], uses piezoelectric clutches to lock the rods. The piezoelectric stacks used in the clutches have high actuation forces but a very small stroke, and a leverage is required to increase the actuator's motion range. Therefore, these clutches cannot be scaled down. The SMA actuated clutch in [27] modulates the stiffness of a CR. However, this design is not suited for the higher payloads required in section locking and requires three cables per section.

In summary, phase transition methods are characterized by long operation times, whereas jamming [25], [28] and tendon locking technologies [26], [29] are not scalable. Thus, here we propose an SMA-driven clutch that overcomes the noted disadvantages of existing solutions. We present a modular, scalable solution for section locking while maintaining a significant clutching force thanks to the usage of beaded cables.

TABLE I
SECTION LOCKING METHODS

Type of Locking	Actuation Method	Rigidizing Method	Ref
Phase Transition	Heat	SMP	[21]
	Heat	LMPA	[22]
Jamming	Cable Tension	Joint friction	[25]
	Pneumatic	Layer jamming	[28]
Tendon Locking	Piezoelectric	Cable clutching	[26]
	Solenoid clutch	Cable clutching	[29]
	SMA	Cable clutching	[27]

The proposed UA CR has four motors and eight cables which could, in theory, control an unlimited number of sections thanks to mechanical clutches to lock cables in independent sections. The clutches are actuated by shape memory alloy (SMA) wires and can be scaled down to navigate in cluttered environments.

Two variants of the UA CR are here proposed: one with smooth (i.e. with constant diameter) actuation cables, and a discrete version with beaded cables, characterized by local cable diameter changes to improve the clutching force thanks to their form factor. Beaded cables are thus able to withstand higher loads and result in a snake robot whose workspace of lockable poses is discrete; this yields interesting problems related to the lockable workspace to be studied. The advantages of the discrete variant include higher accuracy and repeatability, and the finite number of configurations simplifies motion planning and control [30], [31], as less feedback is required. The novel robot with beaded cable is discussed in comparison to the continuous design; their performance is evaluated through kinematic analysis and experimental tests.

II. ROBOT DESIGN

In this section, we introduce a scalable underactuated CR with novel SMA-actuated clutches to enable the independent configuration change of any single section at a given time whilst maintaining the shape of all other sections. With a novel motion strategy, any number of CR sections equipped with the proposed clutch design can be actuated with only four cables.

A. Conceptual design

The proposed CR design requires just two sets of four cables, with two pairs of antagonistic cables per set. The cables run through the entire backbone length to achieve underactuation through SMA-actuated clutches, shown in Fig. 1. The first set of cables, referred to as the *friction cables* and in black in Fig. 1, locks the motion of any sections that is not being actuated. A second set of cables, called *actuation cables* and in cyan in Fig. 1, actuates the motion of the unlocked section(s). Between two consecutive sections i and i+1 of the robot, two sets of clutches are placed to lock actuation and friction cables: actuation clutches $C_{a,i}$ and friction clutches $C_{f,i}$. By locking a set of cables with the clutches both at the top and base of a section, the configuration of that section is fully constrained.

The clutching segment is composed of two disks with slots for clutches which move in the radial direction to clamp cables, as shown in Fig. 2a. The clutch is actuated when a current passes through the SMA wire, making it shrink. The decrease in length of the SMA simultaneously pulls four clutches in the radial direction, thanks to the SMA routing shown in Fig. 2. Each set of clutches has two states: locked or unlocked. All clutches in a set are always in the same state. The entire clutching segment is made by assembling two sets of clutches on top of each other such that their respective SMA wires are offset. The assembly is then closed with external interface disks that connects it to the flexible sections as seen in Fig. 3.

A twin-pivot joint design [32] has been chosen for the flexible sections, as in Fig. 3. Compliant joints were selected to address the twisting problem of continuous backbone CRs and allow an empty internal channel for end-effector delivery.

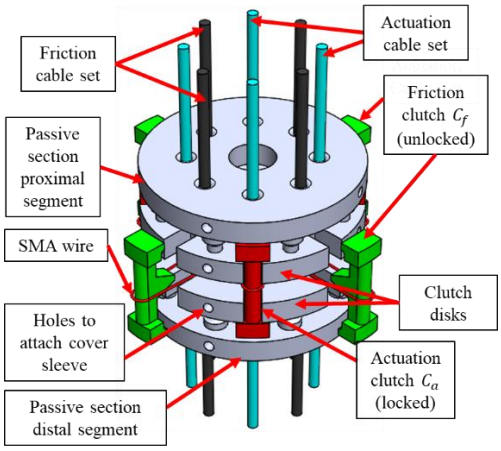

Figure 1: Conceptual design of a SMA-actuated clutching segment: an assembled clutching segment with its two sets of actuation (C_a) and friction (C_f) clutches for the independent locking of actuation and friction cables respectively (locked clutches in red, unlocked clutches in green; clutch motion magnified for visual clarity).

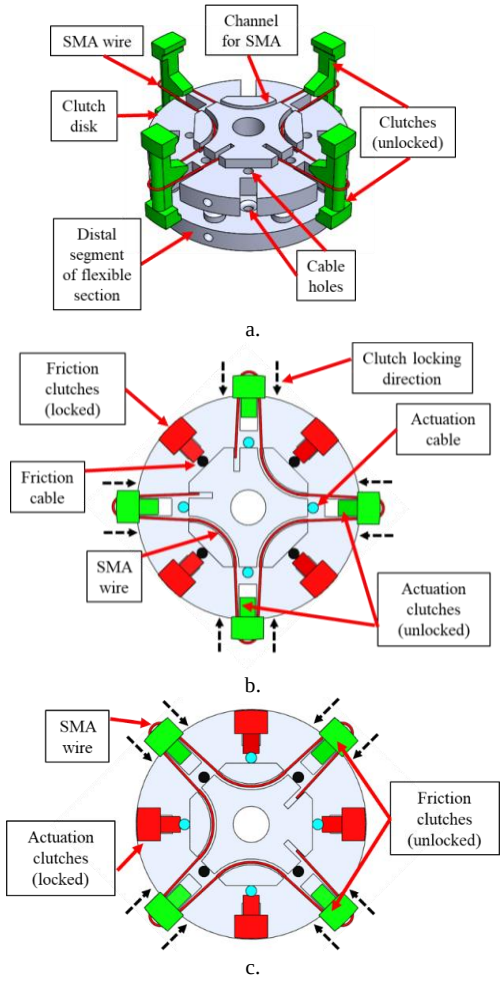

Figure 2: Clutch design: a. Design of a single set of clutches, with the channel for the SMA wire exposed; b. Top view of a clutch with actuation cables unlocked and friction cables locked; c. Top view of a clutch with actuation cables locked and friction cables unlocked.

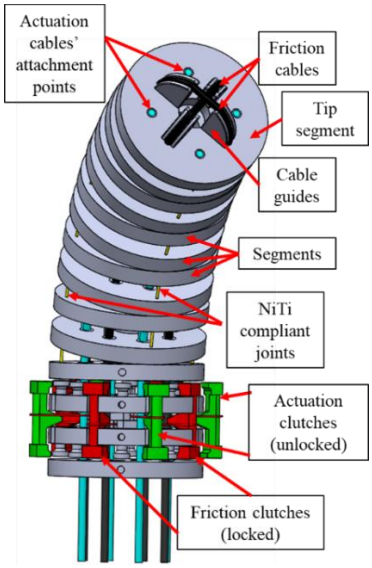

Figure 3: Design solutions of distal passive section with clutching segment. A unique tip guides friction cables across the top. A series of compliant NiTi joint pairs are arranged on perpendicular planes between alternate segments.

While the actuation cables are fixed to the tip of the robot, the friction cables must loop around the tip to release the motion of the distal sections when the proximal sections are locked. For this reason, the proposed tip design enables the compensation of cable shortening on one side with an equivalent lengthening in the antagonistic cable of the pair by sliding across the tip.

This prototype design prioritizes clutching force by routing the SMA cables to pull on the clutches in a radial direction. However, if maximum lumen size and minimum robot diameter are the priorities, the SMA may be routed along the circumference and likewise the friction cables can be routed differently at the tip as not to obstruct the lumen.

B. Motion strategy

The main motion mode of the proposed CR involves a single unlocked section at a time as shown in the example motion sequence in Fig. 4, which follows these steps:

- *First pose:* All the clutches are open, resulting in the straight configuration of the backbone in Fig. 4a.
- *Second pose setup:* The clutches are activated as exemplified in the first row of Table II to move the first section of the robot while locking the second and third.
- *Second pose motion:* The actuation cables are pulled to realize the second desired pose, as in Fig. 4b.
- *Third pose setup:* The clutches are powered on according to the third row of Table II to prepare to move the third section of the robot.
- *Transition time:* A 5 second pause before the next step ensures the SMA wires relax enough to release the actuation cables in the first and second sections.
- *Third pose motion:* The actuation cables are pulled and released to realize the third desired pose, as in Fig. 4c.
- *Further poses:* The previous three steps can be repeated to realize any number of successive poses.

To understand which clutches must be locked for any single section motion, three subsystems of the proposed CR should be considered: the locked proximal sections, a single unlocked section S_i, and the locked distal sections. The locked proximal sections are locked by their friction clutches $C_{f,k}$ up to the unlocked section S_i, i.e., lock $C_{f,k}$ for $k < i$. The locked distal sections are locked by their actuation clutches after the unlocked section S_i, i.e., lock $C_{a,k}$ for $k \geq i$. With these two parts of the robot locked, only the unlocked section S_i is free to move. The general actuation map in Table II reports how the clutches must be activated to independently change the configuration of an individual section. However, any number of unlocked consecutive sections can be controlled simultaneously in continuous bending.

TABLE II
ACTUATION MAP FOR SINGLE SECTION MOTION

To Move:	Lock:	Unlock:
S_1	$C_{a,[1,2]}$	$C_{f,[1,2]}$
S_2	$C_{a,2}$ $C_{f,1}$	$C_{a,1}$ $C_{f,2}$
S_3	$C_{f,[1,2]}$	$C_{a,[1,2]}$
S_i	$C_{a,k}$ for $k \geq i$ $C_{f,k}$ for $k < i$	$C_{a,k}$ for $k < i$ $C_{f,k}$ for $k \geq i$

S = section; C = clutch; a = actuation; f = friction; i = section; k = clutch.

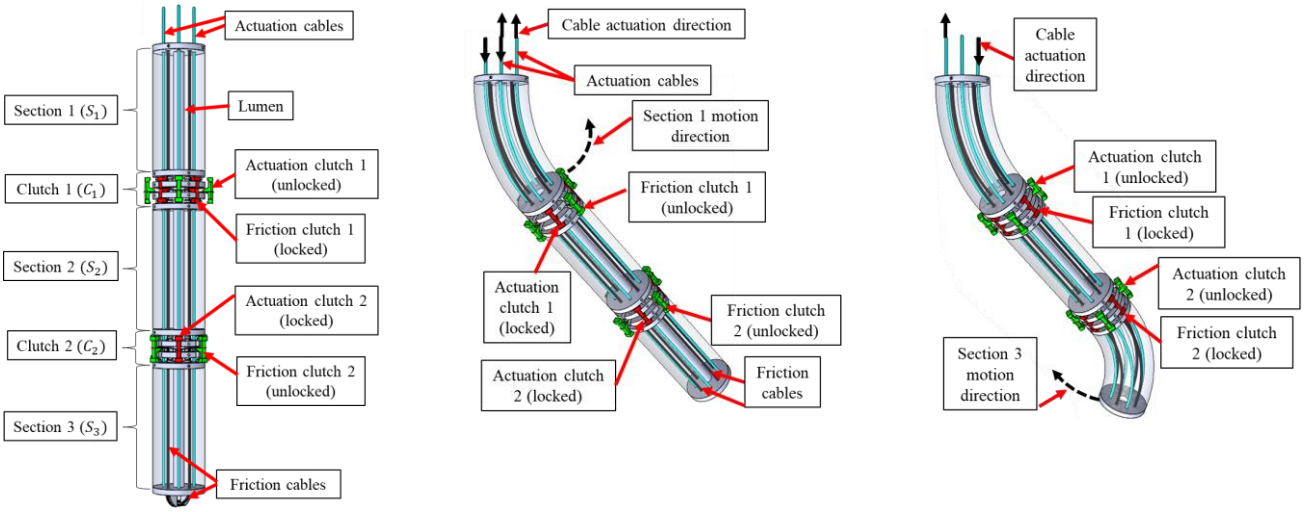

a. b. c.

Figure 4: An example motion sequence: a. Initial (1st) configuration with a straight backbone; b. Intermediate (2nd) configuration, a required passage between the initial and final pose which can be achieved by locking actuation cables with clutches C_1 and C_2 to activate the motion of section S_1 as detailed in the first row of Table II; c. Target (3rd) configuration, achieved by moving section S_3 locking friction cables in both C_1 and C_2 as detailed in the third row of Table II.

C. *Discrete actuation*

The payload of the proposed underactuated CR is limited by the cable tension that its clutches can hold without slipping. By adding beads to the cables at a constant interval throughout their length, as in Fig. 5, the clutching force is increased by the mechanical interference introduced by the beads due to the local diameter increase of the cable. Thus, this method provides a stronger locking force than relying solely on friction.

As consequence of using beaded cables, actuation must be discretised by multiples of the bead pitch to ensure that the clutches always close on a space between beads. Furthermore, the length between the clutches at the base and tip of a section must be a multiple of the bead spacing for the same reason. Using beaded cables results in a discrete workspace of lockable poses. However, unlike existing discrete manipulators based on binary actuations, [33], [34], any section can still operate continuously when held with actuation cable tension.

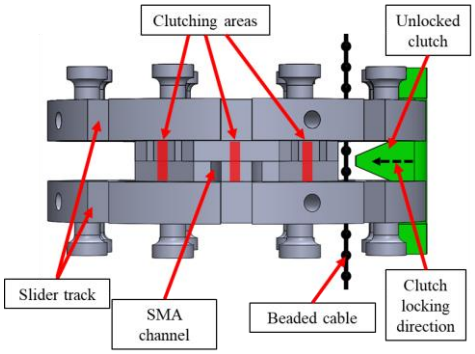

Figure 5: A 3D model of the proposed clutch system with a beaded cable.

III. Robot Analysis

A. *Kinematic modelling*

Cable-driven CRs are usually modelled in the operation, configuration, and actuation spaces, related to the absolute position of the end-effector, the motion angles of each section, and the actuation variables, respectively. In this paper, we adopt a piece-wise constant curvature kinematic model, which models the backbone of the section as a circular arc and defines its configuration with the bending angle θ_i and the direction of bending φ_i [35], with the parameters in Fig. 6 and Table III.

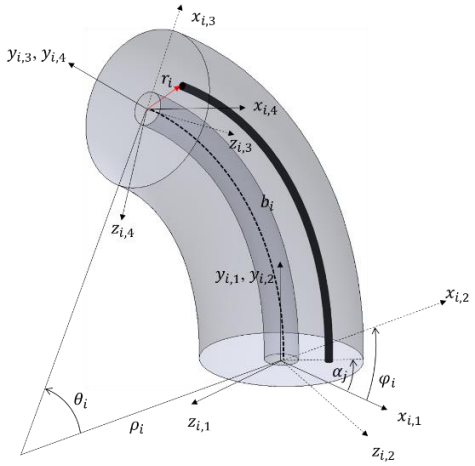

Figure 6: A kinematic diagram of a continuum robot section bending in an arbitrary way, with main design and motion parameters.

TABLE III
KINEMATIC PARAMETERS

Par.	Definition
b_i	Backbone length of the i^{th} section
r_i	Radial distance of cables from center
θ_i	Bending angle of the i^{th} section
φ_i	Direction of bending of the i^{th} section
α_j	Angular position of the j^{th} cable in the cross-section.
$\boldsymbol{P}_n$	Absolute position of the tip of a n-section robot

The kinematics of this class of underactuated CR slightly differs from conventional CRs due to the introduction of rigid clutching segments along the backbone. Thus, the conventional kinematics are adjusted by adding a transformation matrix for each clutch. Given the length along the backbone a_i of the i^{th} clutch, a corresponding translation vector $\mathbf{q_i}$ can be written as

$$\boldsymbol{q_i} = \begin{bmatrix} x_{ci} \\ y_{ci} \\ z_{ci} \end{bmatrix} = \begin{bmatrix} 0 \\ a_i \\ 0 \end{bmatrix} \quad (1)$$

As the clutches do not introduce any rotation, the overall transformation matrix is given by

$$\boldsymbol{C_i} = \begin{bmatrix} \mathbb{1}_{3x3} & \boldsymbol{q_i} \\ \boldsymbol{0_{1\times3}} & \boldsymbol{1_{1\times1}} \end{bmatrix}. \quad (2)$$

Given the constant curvature bending transformation matrix $\boldsymbol{T}_i$ [35] from the proximal to the distal frame of the i^{th} section, an overall transformation matrix can be written as

$$\boldsymbol{P}_n = [\prod_{i=1}^{n} \boldsymbol{T}_i \boldsymbol{C}_i] \begin{bmatrix} \boldsymbol{0_{3\times1}} \\ \boldsymbol{1_{1\times1}} \end{bmatrix}. \quad (3)$$

Once the transformation from configuration to operational space is defined, robot geometry can be used to calculate the length of the cables for a given bend, thus solving the kinematics between configuration and actuation spaces. With reference to the geometry in Fig. 6, we can write the length of a section b_i as a function of its bending angle θ_i as $b_i = \rho_i \theta_i$, where ρ_i is the bending radius of that section. As the bending plane of the portion of cable l_j running through that section is parallel to the bending plane of the section, the cable shares the section's bending angle θ_i, but with a different bending radius. The length of the portion of the cable l_j running through the i^{th} section can be expressed as

$$l_{ij} = b_i + \theta_i r_i \cos(\alpha_j - \varphi_i) \quad (4)$$

where r_i is the distance from the center of the disk to the cable hole and α_j describes the angular position of the j^{th} cable in the cross-section of the robot. By assuming an eight-cable configuration, the cables are defined by $\alpha_j = j\pi/4$, with $j = \{0, 2, 4, 6\}$ for the actuation cable set and $j = \{1, 3, 5, 7\}$ for the friction cable set. The forward kinematics of the i^{th} section can be written as

$$\varphi_i = \alpha_j + \arctan\left(\frac{l_{i(j+2)} - b_i}{l_{ij} - b_i}\right) \quad (5)$$

$$\theta_i = \frac{l_{ij} - b_i}{r_i \cos(\alpha_j - \varphi_i)} \quad (6)$$

In the proposed beaded cable solution, the two sets of clutches always grasp the cables between beads. To ensure clutches always grasp between beads, a relationship is derived from (4) to obtain the bead pitch on the friction cable as a function of the bead pitch on the actuation cable. The cable layout in the proposed design is characterized by writing (4) for $j = \{0, 1, 6\}$, which results in:

$$l_{i1} = l_{i0} \cos\frac{\pi}{4} - l_{i6} \sin\frac{\pi}{4} + b_i \quad (7)$$

Thus, for this example cable arrangement, coordinated motion can be obtained by scaling the bead pitch on the friction cable(s), $j = 1$ by a factor of $\frac{\sqrt{2}}{2}$ of the bead pitch on the actuation cables $j = \{0, 6\}$. Therefore, any discrete actuation in integer multiples of the bead spacing can result in feasible clutching between beads on all cables. Equation (7) is represented visually in Fig. 7 (full derivation in appendix).

Another challenge of the cables is ensuring that the unique "looping" tip design does not compromise the functioning of the robot. Therefore, the added cable length "gained" during bending on one side must be equal to the reduction on the other side. This can be proved for an antagonistic pair of cables in radially opposite positions by rewriting (4) for a generic cable located at α_j and its antagonistic partner at $\alpha_j + \pi$. For any bending angle θ_i, the length variation of both sides of the pair is

$$\Delta = \theta_i r_i \cos(\alpha_j - \varphi_i), \quad (8)$$

thus ensuring a correct functioning of the proposed design.

Conventional inverse kinematic models [36], [37] can be applied to underactuated continuum robots, even if they require unique motion planning (as discussed in Section III-C).

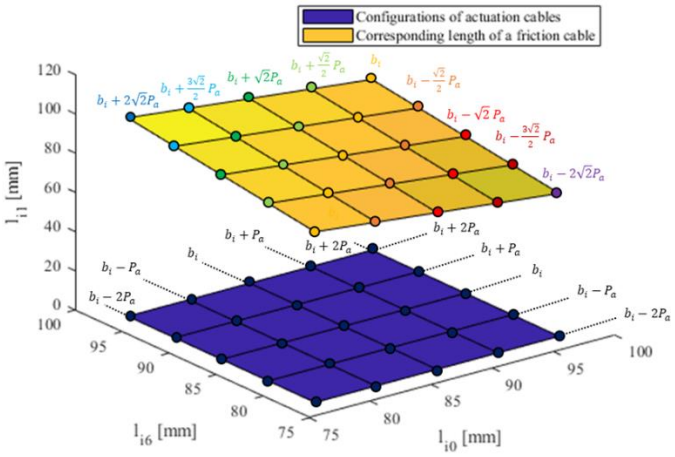

Figure 7: A graphical representation of how bead pitch is scaled to ensure that for each discrete position of the actuation cables, represented as node on the base plane, the friction clutches always clutch between the corresponding beads, whose position is represented as nodes on the upper surface.

B. Continuous and discrete workspace

When using continuous actuation, the workspace of the proposed underactuated CR is, as expected, a continuous dome-shaped volume, as illustrated in Fig. 8a. Conversely, the workspace can be reduced to a discrete set of reachable points when using discrete actuation. By defining the discrete cable lengths for each section as required by the bead spacing, (5-6) are used to find the discretisation in configuration space which is then used in the transformation matrices of (3). The discrete workspace of the example geometry in Table IV can be computed and compared to its continuous counterpart.

TABLE IV
ROBOT GEOMETRY

Parameter	Symbol	Value
Disk outer diameter	d_{out}	38 mm
Disk inner diameter	d_{in}	10 mm
Cable diameter	d_c	0.26 mm
Bead diameter	d_b	0.75 mm
Bead pitch (actuation cable)	P_a	5 ± 1 mm
Bead pitch (friction cable)	P_f	3.53 ± 1 mm
Clutch tip width	κ	2.7 mm
Cable radial position	r	11 mm
Clutch length along the backbone	a_1, a_2, a_3	28, 28, 0 mm
Disk length along the backbone	a_d	4 mm
Number of segments per section	m	11
Exposed NiTi rod length	a_r	4.3 mm
NiTi rod diameter	d_r	0.63 mm

In Fig. 8b, four cross-sections of the workspace, corresponding to the planes in Fig. 8a, show the continuous

workspace as the blue region and reachable discrete poses with red markers. The discrete workspace density is greatest at the tip and most sparse at the edges, due to the non-linear kinematics. This density can be increased by decreasing the bead pitch. Furthermore, the number of points increases exponentially with the number of sections [38]. As the discrete points represent only those poses that are lockable with bead interference, the discrete robot can still move any single section in a continuous manner when held on cable tension alone.

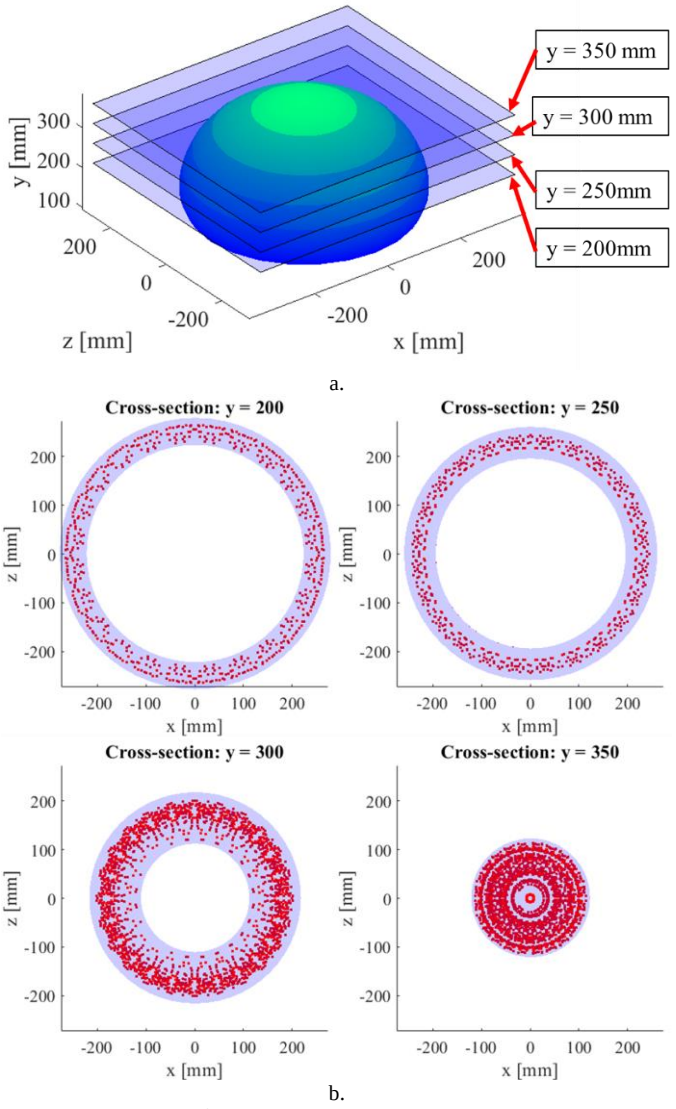

Figure 8: Workspace of the proposed underactuated continuum robot: a. View of the continuous workspace of the robot when using smooth actuation cables; b. Comparison of continuous (blue region) and discrete (red points), when using beaded actuation cables, workspace in the cross-sections of Fig. 8a.

Beaded cables greatly improve the maximum tension that the clutches can hold but introduce a kinematic source of error due to bead pitch tolerance. The corresponding workspace error can be estimated by relating the ratio between a change in cable length $\Delta \boldsymbol{l}$ and the resultant change of the end-effector position $\Delta \boldsymbol{x}$ to the Jacobian matrix, obtained by deriving (3) and (5-6). Yoshikawa's manipulability index is here proposed to give a numerical estimation of the amplification factor between an actuation space error and its corresponding displacement in the operational space [39] as

$$w = \sqrt{|\boldsymbol{J}\boldsymbol{J}^{\boldsymbol{T}}|}, \quad (9)$$

This index, shown in Fig. 9 for a slice of the workspace, can be used to map the effect of the bead pitch error onto the robot's performance in the workspace. As such, this shows that the end-effector error from a 1mm bead pitch error has an upper bound of 5.4mm (1.64% of robot length).

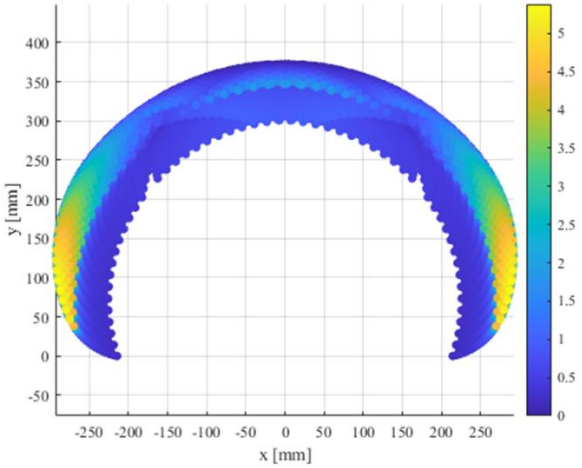

Figure 9: Yoshikawa's manipulability index for a cross-section of the discrete workspace, used as a numerical estimation of the amplification factor between actuation space error and the corresponding error in operational space.

C. Motion planning for underactuated continuum robots

A conventional CR can simultaneously move any section of its backbone to achieve a desired pose. However, the motion strategy of the proposed underactuated CR, outlined in Section II-B, involves intermittently moving individual sections until the desired pose is achieved. Thus, the sequence of motion should be determined to minimize the overall motion time. As reported in the example motion sequence in Fig. 4, a pause between consecutive motions is needed each time a set of clutches changes states. For this reason, the number of state changes that are needed to reach a desired pose from a starting configuration is a key requirement for motion planning.

In Fig. 10, a graphical representation of this information is obtained by plotting in different colors the regions of the workspace that can be reached by moving different sections from a straight configuration (as in Fig. 4a). A cross-section on the XY plane is reported in Fig. 10, as it characterizes the entire workspace thanks to its symmetry around the Y-axis. By moving a single section, the workspace of the robot in Fig. 10 is reduced to three different arcs of points shown in purple and oranges, each characterized by a different active section. Unlocking two sections in sequence expands this workspace to larger areas. Due to the serial nature of the robot, moving a proximal section results in a larger region than the one obtained by moving a distal section; this can be seen in Fig. 10 with the increasing size of the combined workspace 2 & 3 (yellow), 1 & 3 (green), and 1 & 2 (light blue). Finally, there are large dark blue regions of the workspace that can only be reached by moving all the three sections of the robot.

A pseudo-code for motion planning is thus outlined in Table V to identify which sections to move, to go from an initial pose to a desired one and calculate the corresponding change in actuation cable lengths. More intermediate configurations are

required for cluttered environments, analogous to a 3-point turn maneuver in a tight road. The order and number of intermediate configurations can be optimized by minimizing a cost function (e.g. motion time, distance from obstacle, energy efficiency).

TABLE V
ALGORITHM FOR POSE-TO-POSE MOTION

Input

Current pose data = $[l_{i0}^{c}, l_{i2}^{c}]$
Desired pose data = $[l_{i0}^{D}\ l_{i2}^{D}]$
Total number of sections = N
Actuation and friction cables per section = M

Output

Required cable length change for each section = $\boldsymbol{l}$
Index vector of sections to be moved = μ

Algorithm

```
for i = 1:N
    for j = 0:M - 1
        l(i,j) = l_ij^c - l_ij^D
    end
    if abs(sum(l(i,:))) > 0
        μ(i) = TRUE
    else
        μ(i) = FALSE
    end
end
```

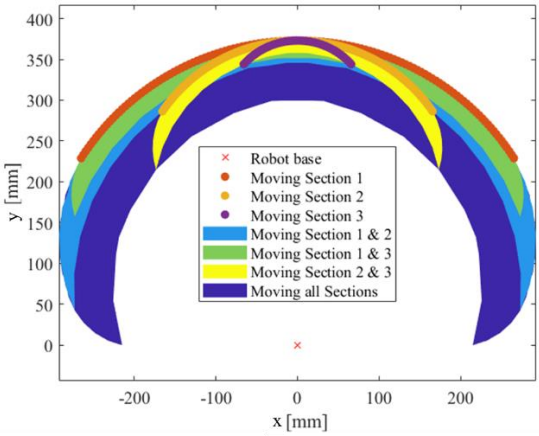

Figure 10: Workspace cross-section divided into reachable areas depending on number of individual/combined sections moved from a straight pose.

IV. PROTOTYPE AND VALIDATION

In this section, the development of a prototype of the proposed underactuated CR is reported. The manufacturing and assembly of the clutch are reported with a thermal calibration to identify the equilibrium working current of the SMA wires. Further design features are discussed as solutions to practical problems such as speeding up the relaxation of the SMA wires, and the main causes of errors in the prototype are discussed. Finally, the motion of a single section is compared to a simulation to determine its accuracy and a motion sequence is realized with a three-section prototype to demonstrate the proposed design.

A. Prototype development

The clutch of the proposed underactuated CR was manufactured according to the design presented in Section II. Different diameters of SMA wires were tested, with larger diameters yielding a higher clutching force and smaller diameters characterized by better flexibility. Furthermore, small diameters also increase the surface area to volume ratio of the wire, resulting in faster relaxation times and lower energy consumption. Overall, a 0.25 mm diameter SMA wire was selected as a trade-off between flexibility, efficiency, bending radius and clutching force. A thin plastic sleeve was added as a cover to the clutching segment to protect it from intruding objects. A clutching segment prototype, in Fig. 11a, was manufactured with a Formlabs Form 3 SLA 3D printer in high temperature resin, for a lightweight design that can endure the temperatures of the SMA wire (up to 105ºC).

To accelerate the phase transition and return the clutch to its unengaged position in a shorter time, a restoring force was introduced by the addition of two elastic bands attached to the top and base of the clutch as shown in Fig. 11a. Furthermore, by preloading the SMA with tension, the elastic bands contribute to an increased clutching force when heated. The preload is obtained by assembling the clutch with the elastic bands and then tensioning the SMA until the clutches fully engage a calibration rod positioned in the holes for the actuation cables. This also ensures that the full stroke of the SMA is available for locking the cables. To improve the scalability of the design, the SMA wire is spooled above the clutch on rollers. This addition to the mechanism ensures that the 5% SMA stroke does not limit the performance of the robot.

A two-step driving current is used to operate the SMA wire: initially, a high current actuates the SMA quickly; a lower current maintains the closed position without overheating the wire. These currents have been calibrated with a thermal camera (Fig. 11b): a high current of 1050mA for 1 second fully contracts a 0.25 mm SMA [40] and 650 mA maintain the SMA in equilibrium at its 70°C activation temperature.

The prototype clutch is further characterised in terms of cable payload and relaxation time. The cable payload is here defined as the amount of tension that can be held by the clutch without the cable slipping when the SMA is at equilibrium temperature. The beaded cables for this prototype were realized with knotted Dyneema® cable (Ultra High Molecular Weight Polyethylene). The highest clutching force of our prototype SMA clutch with knotted Dyneema® was measured at 14 N. Above this value, the knots compress and slip through the clutch. As the robot payload is dependent on the clutching force, applications requiring higher payloads or at a different scale should consider tailored designs (e.g. crimped beads).

Clutch relaxation time is the time between switching off the current and the cable slipping from the grasp of the clutch. For clutches initially at equilibrium temperature, the time is dependent on cable type and payload, as per Fig. 11c. Beaded cables increase relaxation time at low payloads as the clutch must open further to release a bead. Conversely, a higher payload decreases relaxation time as cables with higher tension exerts more force on the SMA, restoring it to its open position faster. The experimental curve in Fig. 11c can be thus used to define an optimal tension for the actuation cables of the robot: an optimal 5 sec transition time between poses for the beaded cable UA CR can be obtained by preloading actuation cables with a tension of 3.7 N or more. While smooth cables enable a 2 sec transition, their maximum cable payload is 1.8 N.

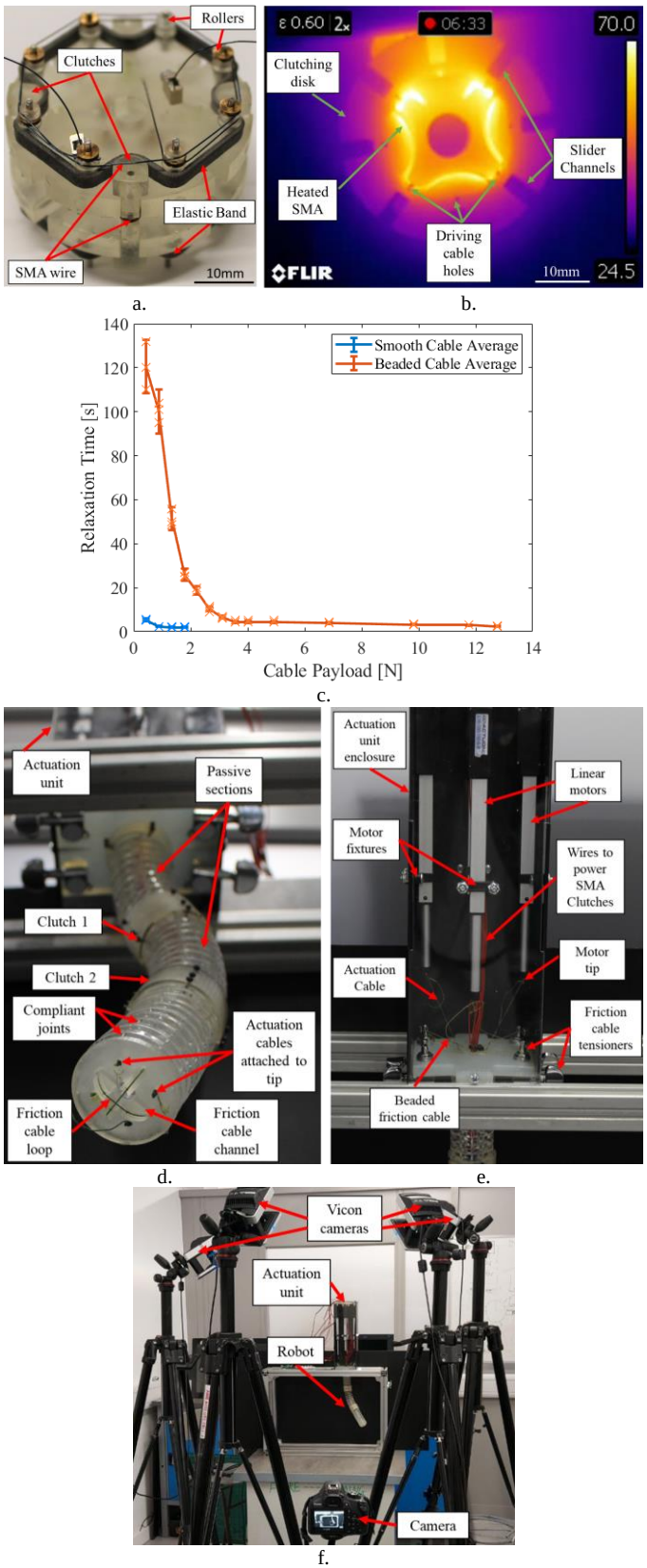

Figure 11: A prototype of the proposed underactuated continuum robot: a. A clutching segment; b. A thermal camera infrared image of a 0.25 mm SMA at its thermal equilibrium inside a clutch prototype; c. Clutch relaxation time as a function of cable type and tension; d. A three-section underactuated continuum robot prototype with SMA clutches; e. Main elements of the actuation unit; f. Experimental setup with a VICON motion tracking system.

The remaining components of the prototype have been manufactured to assemble the body of the underactuated CR as in Fig. 11d. The vertebrae of the flexible sections have been laser-cut from acrylic Perspex, and the slots for the NiTi joints of the backbones have been drilled. An actuation unit was assembled from laser-cut Perspex with commercial linear servomotors (Actuonix L16R) as shown in Fig. 12e.

B. Experimental validation

To calculate the accuracy of the underactuated CR, a VICON motion capture system with 4 Vantage cameras, calibrated to an accuracy of 0.05 mm, has been set up as in Fig. 11f. The position of the tip section has been measured and compared to a simulation for large and small tip oscillations between 0.91 radians and 0.45 radians respectively. As reported in Fig. 12a, an absolute position error of 3 mm, corresponding to 3.5% of the section length, has been measured for the prototype.

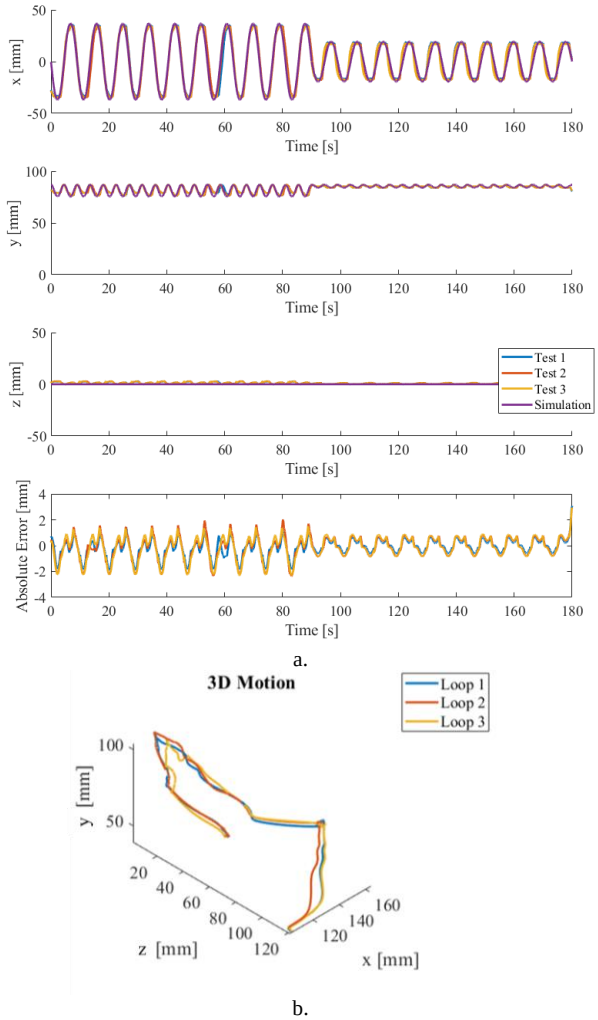

Figure 12: Experimental results: a. Cartesian position of the section tip over time for a repeated motion, with data from three repetition and a simulation reported; b. Position of the tip point of a three-section robot during three motion sequences as acquired by the Vicon motion capture system.

The UA motion strategy is further validated by an example motion sequence with the steps in Fig. 13 and Table VI:

- *First pose:* The cables are tensioned, and the clutches locked, while the robot is in a straight configuration.
- *Second pose setup:* The clutches are powered according to

the second row of Table II to move the second section of the robot while locking the first and third ones. An interval of 5 seconds ensures the relaxation of the relevant clutches.

- *Second pose motion:* The actuation cables are moved by the linear motors to realize the second desired pose.
- *Third pose setup:* The clutches are powered according to the first row of Table II to move the first section of the robot. The transition time of 5 seconds is required.
- *Third pose motion:* The actuation cables are moved by the linear motors to realize the third desired pose.
- *Further poses:* The previous two steps can be repeated to realize any number of successive poses.

The motion of the tip of the robot was acquired over three iterations by the Vicon motion capture system as shown in Fig. 12b. The average repeatability of the end-effector is 1.41 mm, corresponding to 0.43% of the backbone. The most significant source of error is due to bead pitch tolerance, as the cables were manually knotted. The consequence of this tolerance is estimated by an amplification factor in the robot analysis section. Alternative procedures, such as using crimp beads instead of knots, are currently being investigated to automate the procedure and reduce this error.

TABLE VI
POSE CONFIGURATION PARAMETERS

POSE	θ_1	φ_1	θ_2	φ_2	θ_3	φ_3
1	0°	0°	0°	0°	0°	0°
2	0°	0°	45°	45°	0°	0°
3	25°	225°	45°	45°	0°	0°

V. CONCLUSION

The structure of cable-driven CRs makes them ideally suited to navigating complex environments such as aeroengines, nuclear reactors and in search and rescue operations. However, they are restricted by bulky actuation packs, which hinder deployment, and their many cables, which put an upper limit on their length. Furthermore, conventional CRs are not modular and, once assembled, their length cannot be modified, as their actuation is not designed to accommodate additional motors.

As such, underactuated CRs with lockable sections have been identified as a solution to the noted disadvantages of cable-driven CRs but are currently limited by their long operating times and/or by non-scalable designs. In this paper, SMA clutches are introduced as a cable-locking method which is light, scalable, and inexpensive. In the proposed design, two sets of cables and clutches achieve independent configuration changes of any number of sections with just four actuating motors. The key results of this work can be summarized as:

- *Novel underactuated continuum robot:* A scalable clutch design is proposed for section locking with SMA clutches.
- *Motion strategy:* A clutch configuration map is proposed to achieve any succession of poses with the proposed robot.
- *Discrete actuation*: Beaded cables are reported as a solution to increase payload and repeatability. Design guidelines are provided to find optimal parameter values.
- *Workspace analysis:* The workspace of the discrete robot with beaded cables is modelled and compared to that of its continuous twin. The influence of the bead pitch on the workspace is analyzed, with the discrete workspace converging to a continuous workspace when increasing the number of sections and/or decreasing bead pitch.
- *Demonstration:* A prototype of the proposed robot is manufactured and moved through a series of poses to estimate its performance, achieving a repeatability of 0.43% of its backbone length. The accuracy of the distal section is measured as 3.5% of a section length when compared to its CCK simulation.

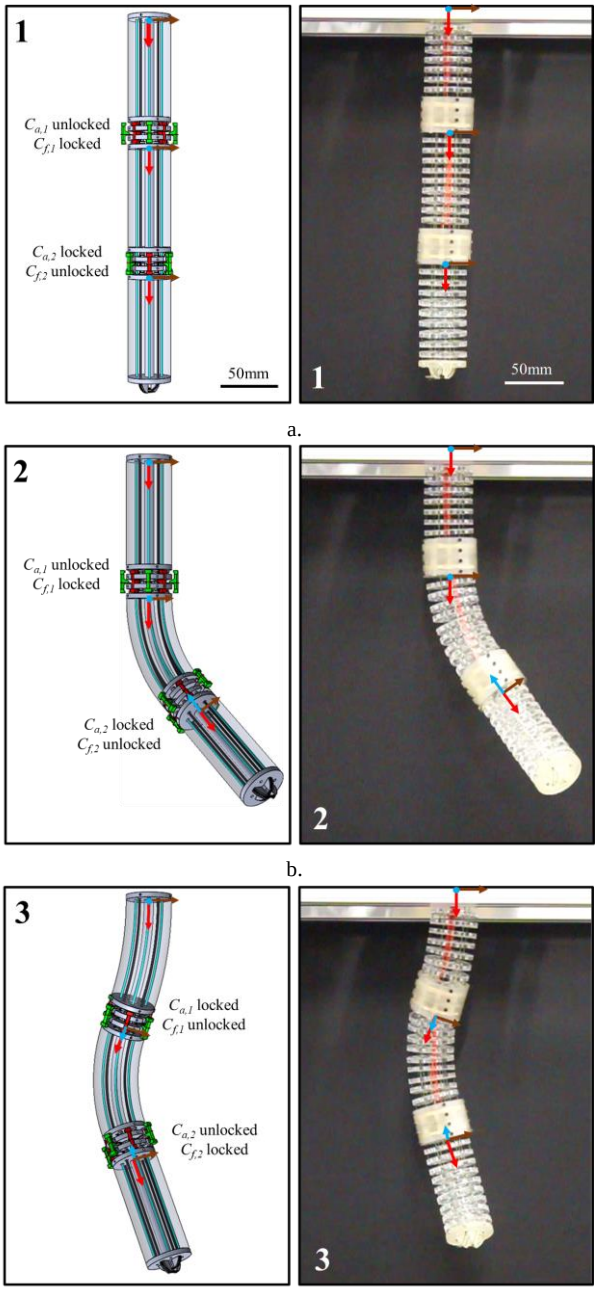

Figure 13: Motion test with the proposed underactuated continuum robot performing a sequence poses, with a simulation of the motion in a 3D CAD software and the corresponding motion performed by the robot prototype: a. First pose; b. Second pose; c. Third pose.

When compared to existing designs, the advantages of the proposed underactuated CR can be identified as:

- *Speed*: SMA clutches lock sections in 1 second and can unlock a section in 5 seconds, faster than any other scalable underactuated CRs in scientific literature to date.
- *Simple control*: Position sensors are not required due to the discrete nature of the actuation and cables, and a kinematic mapping of all the possible positions reduces inverse kinematics to a simple search.
- *Reliability*: By engaging the beads with the clutches, cable slipping can be prevented, and the position of the end effector is always known within a known error.
- *Lightweight*: SMA wire clutches are lightweight in comparison to technologies with phase changing materials, limiting the undesired bending of the CR's backbone under its own weight and improving robot portability.
- *Scalability*: As the size of the clutch mainly depends on the mechanical design of the slider, the dimensions of the clutch can be scaled down for miniaturized designs.
- *Modularity:* The number of sections can be increased by assembling new flexible sections and clutches onto the robot's base without changing the actuation unit.

In conclusion, thanks to its simple control and flexible design, this novel underactuated system represents a valuable low-cost alternative to conventional CRs for inspection, maintenance, repair, and service tasks.

In future work, an optimal path planning algorithm for reaching points in a cluttered environment with minimum intermediate configurations will be introduced for the proposed class of underactuated continuum robots.

APPENDIX A

For our prototype cables are arranged with $\alpha_j = j\pi/4$, with $j = \{0, 2, 4, 6\}$ for the actuation cable set and $j = \{1, 3, 5, 7\}$ for the friction cable set. Equation (4) gives the length of a general cable l_{ij} at angular position α_j. Writing (4) for a cable located on the x axis ($\alpha_j = 0, j = 0$) results in

$$l_{i0} = b_i + \theta_i r_i \cos(-\varphi_i), \tag{10}$$

whereas, for the actuation cable that is located perpendicular to the one of the x axis ($\alpha_j = \frac{3}{2}\pi$, j=6), we obtain

$$l_{i6} = b_i + \theta_i r_i \cos\left(\frac{3}{2}\pi - \varphi_i\right) \tag{11}$$

Dividing (11) by (10) gives

$$\frac{l_{i6} - b_i}{l_{i0} - b_i} = \frac{cos\left(\frac{3}{2}\pi - \varphi_i\right)}{cos(-\varphi_i)} \tag{12}$$

By using the trigonometric identity for cosine subtraction, (12) becomes

$$\frac{l_{i6} - b_i}{l_{i0} - b_i} = \frac{\cos\left(\frac{3}{2}\pi\right)\cos(\varphi_i) + \sin(\frac{3}{2}\pi)\sin(\varphi_i)}{\cos(\varphi_i)} = -\tan(\varphi_i). \tag{13}$$

Dividing (4) for a general cable at any angular position α_j by (10) for a cable on the x axis, gives

$$\frac{l_{ij} - b_i}{l_{i0} - b_i} = \cos(\alpha_j) + \sin(\alpha_j)\tan(\varphi_i) \tag{14}$$

Substituting our result from (13) into (14) shows us that

$$\frac{l_{ij} - b_i}{l_{i0} - b_i} = \cos(\alpha_j) + \sin(\alpha_j)\left(\frac{b_i - l_{i6}}{l_{i0} - b_i}\right) \tag{15}$$

Rearranging and simplifying (15) leads us to a result which expresses the length general cable l_{ij} in terms of the two perpendicular actuation cables (l_{i0}, l_{i6}):

$$l_{ij} = \sin(\alpha_j)(b_i - l_{i6}) - \cos(\alpha_j)(l_{i0} - b_i) + b_i \tag{16}$$

Notice that this more general equation (16) becomes (7) when j = 1 and $\alpha_j = j\pi/4$, which defines the location of our first friction cable. The above steps may be repeated for other pairs of actuation cables. For example, for (l_{i0}, l_{i2}) we obtain

$$l_{ij} = \sin(\alpha_j)(l_{i2} - b_i) + \cos(\alpha_j)(l_{i0} - b_i) + b_i \tag{17}$$

REFERENCES

[1] M. Wang, X. Dong, W. Ba, A. Mohammad, D. Axinte, and A. Norton, "Design, modelling and validation of a novel extra slender continuum robot for in-situ inspection and repair in aeroengine," *Robot. Comput. Integr. Manuf.*, vol. 67, Feb. 2021.

[2] X. Dong *et al.*, "Continuum Robots Collaborate for Safe Manipulation of High-Temperature Flame to Enable Repairs in Challenging Environments," *IEEE/ASME Trans. Mechatronics*, pp. 1–4, 2022.

[3] A. Mohammad, M. Russo, Y. Fang, X. Dong, D. Axinte, and J. Kell, "An efficient follow-the-leader strategy for continuum robot navigation and coiling," *IEEE Robot. Autom. Lett.*, 2021.

[4] M. Russo, N. Sriratanasak, W. Ba, X. Dong, A. Mohammad, and D. Axinte, "Cooperative Continuum Robots: Enhancing Individual Continuum Arms by Reconfiguring Into a Parallel Manipulator," *IEEE Robot. Autom. Lett.*, vol. 7, no. 2, pp. 1558–1565, Apr. 2022.

[5] J. Burgner-Kahrs, D. C. Rucker, and H. Choset, "Continuum Robots for Medical Applications: A Survey," *IEEE Trans. Robot.*, vol. 31, no. 6, pp. 1261–1280, Dec. 2015.

[6] D. B. Camarillo, C. F. Milne, C. R. Carlson, M. R. Zinn, and J. K. Salisbury, "Mechanics modeling of tendon-driven continuum manipulators," *IEEE Trans. Robot.*, vol. 24, no. 6, pp. 1262–1273, 2008.

[7] M. Jha and N. R. Chauhan, "A review on Snake-like Continuum Robots for Medical Surgeries," in *IOP Conference Series: Materials Science and Engineering*, 2019, vol. 691, no. 1, p. 012093.

[8] J. S. Mehling, M. A. Diftler, M. Chu, and M. Valvo, "A minimally invasive tendril robot for in-space inspection," in *Proceedings of the First IEEE/RAS-EMBS International Conference on Biomedical Robotics and Biomechatronics, 2006, BioRob 2006*, 2006, vol. 2006, pp. 690–695.

[9] E. Amanov, T.-D. Nguyen, and J. Burgner-Kahrs, "Tendon-driven continuum robots with extensible sections—A model-based evaluation of path-following motions:," *https://doi.org/10.1177/0278364919886047*, vol. 40, no. 1, pp. 7–23, Nov. 2019.

[10] M. Russo, L. Raimondi, X. Dong, D. Axinte, and J. Kell, "Task-oriented optimal dimensional synthesis of robotic manipulators with limited mobility," *Robot. Comput. Integr. Manuf.*, vol. 69, p. 102096, Jun. 2021.

[11] M. B. Pritts and C. D. Rahn, "Design of an artificial muscle continuum robot," in *Proceedings - IEEE International Conference on Robotics and Automation*, 2004, vol. 2004, no. 5, pp. 4742–4746.

[12] Y. Goergen *et al.*, "Shape memory alloys in continuum and soft robotic applications," *ASME 2019 Conf. Smart Mater. Adapt. Struct. Intell. Syst. SMASIS 2019*, Dec. 2019.

[13] P. E. Dupont, J. Lock, B. Itkowitz, and E. Butler, "Design and control of concentric-tube robots," *IEEE Trans. Robot.*, vol. 26, no. 2, pp. 209–225, Apr. 2010.

[14] H. B. Gilbert, D. C. Rucker, and R. J. W. III, "Concentric Tube Robots: The State of the Art and Future Directions," *Springer Tracts Adv. Robot.*, vol. 114, pp. 253–269, 2016.

[15] V. Modes and J. Burgner-Kahrs, "Calibration of Concentric Tube Continuum Robots: Automatic Alignment of Precurved Elastic Tubes," *IEEE Robot. Autom. Lett.*, vol. 5, no. 1, pp. 103–110, Jan. 2020.

[16] I. D. Walker, H. Choset, and G. S. Chirikjian, "Snake-Like and Continuum Robots," *Springer Handb. Robot.*, pp. 481–498, Jan. 2016.

[17] I. D. Walker, "Continuous Backbone 'Continuum' Robot

Manipulators," *ISRN Robot.*, vol. 2013, pp. 1–19, Jul. 2013.
[18] M. Mahvash and P. E. Dupont, "Stiffness control of surgical continuum manipulators," *IEEE Trans. Robot.*, vol. 27, no. 2, pp. 334–345, Apr. 2011.
[19] R. E. Goldman, A. Bajo, and N. Simaan, "Compliant motion control for continuum robots with intrinsic actuation sensing," in *Proceedings - IEEE International Conference on Robotics and Automation*, 2011, pp. 1126–1132.
[20] Z. Jiang, Y. Luo, and Y. Jin, "New cable-driven continuun robot with only one actuator," in *2017 IEEE International Conference on Cybernetics and Intelligent Systems, CIS 2017 and IEEE Conference on Robotics, Automation and Mechatronics, RAM 2017 - Proceedings*, 2018, vol. 2018-Janua, pp. 693–698.
[21] A. Firouzeh, S. S. Mirrazavi Salehian, A. Billard, and J. Paik, "An under actuated robotic arm with adjustable stiffness shape memory polymer joints," *Proc. - IEEE Int. Conf. Robot. Autom.*, vol. 2015-June, no. June, pp. 2536–2543, 2015.
[22] F. Alambeigi, R. Seifabadi, and M. Armand, "A continuum manipulator with phase changing alloy," in *Proceedings - IEEE International Conference on Robotics and Automation*, 2016, vol. 2016-June, pp. 758–764.
[23] Y. Fang, C. Bishop, W. Ba, J. B. Díez, A. Mohammad, and X. Dong, "A Universal Stiffening Sleeve Designed for All Types of Continuum Robot Systems," in *Lecture Notes in Computer Science (including subseries Lecture Notes in Artificial Intelligence and Lecture Notes in Bioinformatics)*, 2020, vol. 12228 LNAI, pp. 15–24.
[24] I. W. Hunter, S. Lafontaine, J. M. Hollerbach, and P. J. Hunter, "FAST REVERSIBLE NITI FIBERS FOR USE IN MICROROBOTICS," *IEEE Micro Electro Mech. Syst.*, vol. 91, pp. 166–170, Jan. 1991.
[25] A. Degani, H. Choset, A. Wolf, and M. A. Zenati, "Highly articulated robotic probe for minimally invasive surgery," in *Proceedings - IEEE International Conference on Robotics and Automation*, 2006, vol. 2006, pp. 4167–4172.
[26] B. Kang, R. Kojcev, and E. Sinibaldi, "The First Interlaced Continuum Robot, Devised to Intrinsically Follow the Leader," *PLoS One*, vol. 11, no. 2, p. e0150278, Feb. 2016.
[27] C. Yang *et al.*, "Geometric constraint-based modeling and analysis of a novel continuum robot with Shape Memory Alloy initiated variable stiffness," *Int. J. Rob. Res.*, vol. 39, no. 14, pp. 1620–1634, 2020.
[28] Y. J. Kim, S. Cheng, S. Kim, and K. Iagnemma, "Design of a tubular snake-like manipulator with stiffening capability by layer jamming," in *IEEE International Conference on Intelligent Robots and Systems*, 2012, pp. 4251–4256.
[29] Y. Zuo, G. Merritt, and X. Wang, "Design of a Novel Surgical Robot with Rigidity-Adjustable Joints based on Time-Division Multiplexing Actuation," in *Proceedings of the IEEE RAS and EMBS International Conference on Biomedical Robotics and Biomechatronics*, 2020, vol. 2020-Novem, pp. 885–890.
[30] G. S. Chirikjian, "Binary paradigm for robotic manipulators," *Proc. - IEEE Int. Conf. Robot. Autom.*, no. pt 4, pp. 3063–3069, 1994.
[31] G. S. Chirikjian, "Inverse Kinematics of Binary Manipulators Using a Continuum Model," in *Journal of Intelligent and Robotic Systems 1997 19:1*, 1997, vol. 19, no. 1, pp. 5–22.
[32] X. Dong, M. Raffles, S. Cobos-Guzman, D. Axinte, and J. Kell, "A Novel Continuum Robot Using Twin-Pivot Compliant Joints: Design, Modeling, and Validation," *J. Mech. Robot.*, vol. 8, no. 2, Apr. 2016.
[33] Y. Miao, F. Gao, and Y. Zhang, "Gait fitting for snake robots with binary actuators," *Sci. China Technol. Sci. 2013 571*, vol. 57, no. 1, pp. 181–191, Nov. 2013.
[34] V. A. Sujan and S. Dubowsky, "Design of a Lightweight Hyper-Redundant Deployable Binary Manipulator," *J. Mech. Des.*, vol. 126, no. 1, pp. 29–39, Jan. 2004.
[35] I. Robert J. Webster and B. A. Jones, "Design and Kinematic Modeling of Constant Curvature Continuum Robots: A Review:," *http://dx.doi.org/10.1177/0278364910368147*, vol. 29, no. 13, pp. 1661–1683, Jun. 2010.
[36] S. Neppalli, M. A. Csencsits, B. A. Jones, and I. D. Walker, "Closed-form inverse kinematics for continuum manipulators," *Adv. Robot.*, vol. 23, no. 15, pp. 2077–2091, 2009.
[37] C. Della Santina, C. Duriez, and D. Rus, "Model Based Control of Soft Robots: A Survey of the State of the Art and Open Challenges," pp. 1–69, 2021.
[38] M. Russo, J. Barrientos-Diez, and D. Axinte, "A kinematic coupling mechanism with binary electromagnetic actuators for high-precision positioning," *IEEE/ASME Trans. Mechatronics*, 2021.
[39] T. Yoshikawa, "Manipulability and redundancy control of robotic mechanisms," *Proc. - IEEE Int. Conf. Robot. Autom.*, pp. 1004–1009, 1985.
[40] "Dynalloy Flexinol Actuator Wires datasheet."

Christopher Bishop received the B.Sc degree in Physics with a Year in Industry from the University of Nottingham in 2019. In 2018 he was a research intern at Nottingham Scientific Limited (NSL), working on processing GNSS signals for precise positioning of receivers. Since 2019, he has been a PhD researcher within the Department of Mechanical, Materials and Manufacturing Engineering at the Rolls-Royce University Technology Centre (UTC) in manufacturing and on-wing technology at the University of Nottingham. His research interests include continuum robots, underactuated mechanisms and inspection and repair robotics.

Matteo Russo (M'18) received the B.Sc., M.Sc. and Ph.D. degrees in mechanical engineering from the University of Cassino, Italy, in 2013, 2015, and 2019, respectively. Between 2015 and 2017 he was a visiting researcher at RWTH Aachen University, University of the Basque Country and Tokyo Institute of Technology. Since 2019, he is a Research Fellow at the Rolls-Royce UTC in Manufacturing and On-Wing Technology, University of Nottingham, Nottingham, UK. His main research interests are continuum robots, robot kinematics and parallel manipulators.

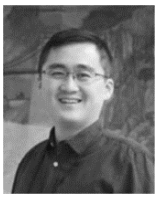

Xin Dong received his B. Eng. Degree in mechanical engineering from Dalian University of Technology, Dalian, China 2008, the M. Eng and PhD degrees in Mechatronics, Robotics and Automation Engineering from Beihang University, Beijing, China in 2011 and from University of Nottingham, Nottingham, UK, 2015.

He is currently an Assistant Professor working at the University of Nottingham. His research interests are extra slender continuum robot and reconfigurable hexapod robots with novel actuation solutions for the application in Aerospace, Nuclear, Oil & Gas, Marine and rescue.

Dragos Axinte received the M.Eng. degree in manufacturing engineering in 1988, and the Ph.D. degree in manufacturing engineering in 1996.

After graduating, he worked in R&D in industry for 10 years and then moved to academia to lead research in the field of machining, process monitoring and design of innovative tooling/robotics for in-situ repair especially related to on-wing repair of aeroengines.

Currently, he is Professor of Manufacturing Engineering at University of Nottingham and Director of Rolls-Royce University Technology Centre (UTC) in Manufacturing and On-Wing Technology.